JOURNAL OF GEOPHYSICAL RESEARCH, VOL. 104, NO. D22, PAGES 27,719-27,734, NOVEMBER 27, 1999

# Mapping net primary production and related biophysical variables with remote sensing: Application to the BOREAS region

Scott J. Goetz, Stephen D. Prince, Samuel N. Goward, Michelle M. Thawley, Jennifer Small, and Andrew Johnston

Laboratory for Global Remote Sensing Studies, Department of Geography, University of Maryland at College Park

**Abstract.** Maps of net and gross primary production, autotrophic respiration, biomass, and other biophysical variables were generated for $10^5$ km$^2$ of boreal forest in central Canada (the Boreal Ecosystem-Atmosphere (BOREAS) region) using a production efficiency model (PEM) driven with remotely sensed observations at 1 km$^2$ spatial resolution. The PEM was based on carbon yields of absorbed photosynthetically active radiation for both gross and net primary production (GPP and NPP), accounting for environmental stress and autotrophic respiration ($R_a$). Physiological control was modeled using remotely sensed maps of air temperature, vapor pressure deficit, and soil moisture. The accuracy of the inferred variables was generally within 10-30% of point measurements at the surface and independent model results (both at the stand level). Biomass maps were derived from visible reflectance measurements and were also compared to independently derived maps. Area-averaged GPP was 604 g C m$^{-2}$ yr$^{-1}$ compared with average canopy respiration of 428 g C m$^{-2}$ yr$^{-1}$ and NPP of 235 g C m$^{-2}$ yr$^{-1}$. Net annual carbon uptake in net primary production for the region totaled 175 teragrams. Canopy carbon exchange (GPP and $R_a$) differed widely between land cover types even though the model does not use land cover information. Extensive areas of the least productive cover types (e.g., lowland needleleaf species) accounted for the greatest amount of NPP.

## 1. Introduction

The carbon balance of the boreal forest biome has attracted much attention in recent years as a result of indirect evidence for a large net atmospheric $CO_2$ sink located in the higher latitudes of the Northern Hemisphere [*Sellers et al.*, 1990; *Tans et al.*, 1990; *Ciais et al.*, 1995; *Denning et al.*, 1995; *Keeling et al.*, 1995; *Fan et al.*, 1998]. There are also suggestions of ecosystem response to global climatic warming in the form of changes in carbon balance associated with deep soil thaw [*Goulden et al.*, 1998] and increased growing season length [*Keeling et al.*, 1996; *Goulden et al.*, 1996; *Myneni et al.*, 1997]. Each of these topics are debated in the scientific community and monitored by policy makers.

Field experiments designed to test the scientific credibility of these issues include the Boreal Ecosystem-Atmosphere Study (BOREAS), an interdisciplinary program intended to quantify the energy, mass, and momentum fluxes of the boreal forest in central Canada. Data collected as part of the BOREAS field campaigns have enabled explicit parameterization of ecophysiological models that simulate the control of vegetation on, for example, carbon and energy fluxes [*Bonan et al.*, 1997; *Frolking*, 1997; *Kimball et al.*, 1997]. Measurements of net primary production (NPP, the difference between gross primary production (GPP) and autotrophic respiration ($R_a$)) and net ecosystem exchange (NEE, including microbial respiration) at several intensively instrumented sites in the BOREAS region have shown large inter-annual variability in both NPP and NEE [*Baldocchi and Vogel*, 1996; *Black et al.*, 1996; *Goulden et al.*, 1997]. These observations were made in small field study sites and, without explicit spatial modeling, cannot be used to assess regional- to global-scale boreal forest carbon budgets.

Spatial extrapolation of point measurements using maps of vegetation types is problematic because of the great landscape heterogeneity of the boreal forest. Simple assignment of carbon fluxes to land cover classes is impractical because of ambiguities in land cover classification, the availability of very few point measurements, large local spatial variability in vegetation cover types, and the temporal variability of land cover change owing to frequent disturbance events (e.g., fire and insect defoliation). Although ecosystem simulation models frequently rely on land cover parameterization, they rarely include information on land use or land cover change [e.g., *Xiao et al.*, 1998] and are severely limited when the land cover consists of anything other than extensive, uniform patches of a few distinct cover types.

Our methodology differs from previous approaches in that we model plant carbon fluxes (GPP and $R_a$) and storage (NPP) at relatively fine spatial resolution (1 km$^2$) over large areas using spatially and temporally contiguous satellite observations. This approach, which we refer to as a production efficiency model (PEM), is relatively new (described below). PEMs, which include models other than ours [e.g., *Potter et al.*, 1993; *Ruimy et al.*, 1994], complement more complex carbon flux models that use field measurements of biophysical variables [e.g., *Kimball et al.*, 1997; *Xiao et al.*, 1998] and hybrid models that use satellite observations of canopy light



Paper number 1999JD900269.
0148-0227/991999/JD900269$09.00

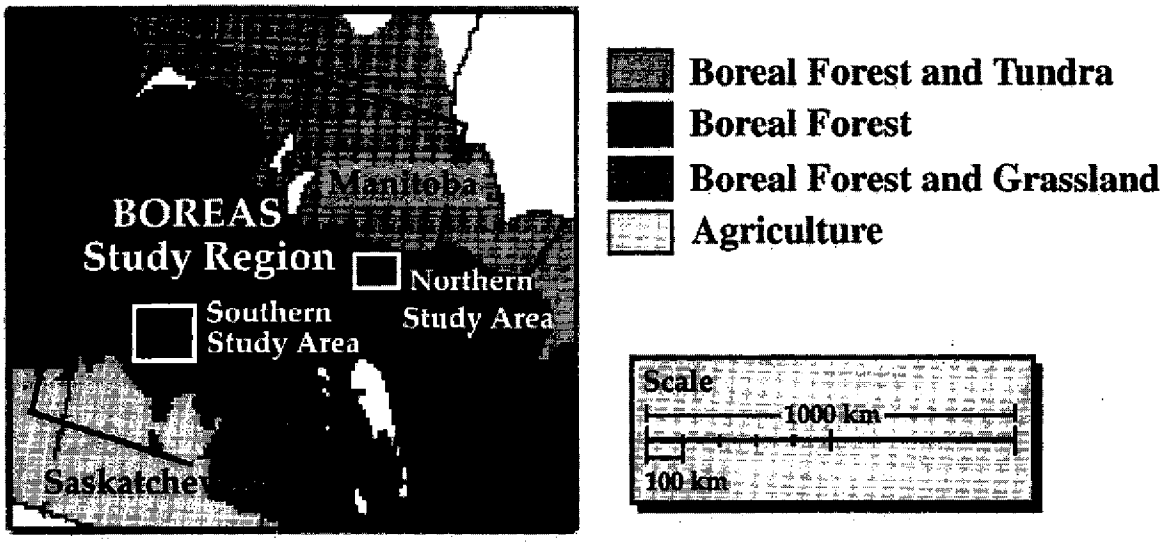


**Figure 1.** Boreal Ecosystem-Atmosphere Study (BOREAS) region in central Canada encompassing a 1000 by 1000 km area bounded by Hudson Bay in the upper right and the U.S. border in the lower left portion of the image.

absorption and point measurements of biophysical variables [e.g., *Foley et al.*, 1996; *Running and Hunt*, 1993].

Our objectives were to apply a primary production model, driven with remotely sensed observations, to the BOREAS study region in order to (1) develop maps of surface environmental variables and canopy carbon fluxes ($CO_2$ assimilation and autotrophic respiration), (2) compare the modeled results at daily and annual timescales with extensive near-surface measurements and other ecosystem model simulations, and (3) provide estimates of net plant carbon exchange (NPP) for the region as a whole.

## 2. Study Area

The BOREAS study region encompasses a $10^6$ km$^2$ (1000 x 1000 km) area of central Canada bounded by 51°-60°N latitude and 94°-111°W longitude (Figure 1). Land cover types follow a temperature and growing season length gradient, ranging from agriculture in the southwest to tundra in the northeast. Soil development varies greatly throughout the region, mainly determined by microtopography and glacial history. Depth to permafrost follows the southwest-northeast gradient across the region and also varies greatly with changes in microtopography. The principal land cover types are fens, bogs, black spruce (*Picea mariana*) and larch (*Larix laracina*) stands on poorly drained, lowland sites, jack pine (*Pinus banksiana*) and paper birch (*Betula papyrifera*) on sandy uplands, quaking aspen (*Populus tremuloides*) and white spruce (*Picea glauca*) on mesic, well-developed soils, and a range of mixed composition stands on intermediate sites. Fire has an important role in boreal landscape dynamics with historical recurrence intervals averaging ~100 years [*Heinselman*, 1973] but increased frequency resulting from human activities and climate warming [*Kasischike et al.*, 1995]. Fires were a frequent occurrence during BOREAS, to the extent that smoke and particulate haze affected substantial portions of the satellite observational record.

## 3. Data

Advanced very high resolution radiometer (AVHRR) local area coverage (LAC) satellite observations, with a nominal nadir resolution of 1.1 km$^2$, were acquired for the study region for 34 days between April 16 and September 7, 1994. Radiometric calibration and geographic registration of the AVHRR data were undertaken by the Canadian Center for Remote Sensing [*Cihlar et al.*, 1997; *Czajkowski et al.*, 1997a]. Mapping of the data to an Albers equal-area conic projection resulted in resampling of the image cells to a uniform 1 km$^2$ resolution. Satellite overpass (acquisition) times ranged from 2200 - 2340 UT. Correction for attenuation of the near-infrared (NIR) channel by atmospheric water vapor was carried out using a split-window estimation of atmospheric precipitable water vapor (described in section 4). No atmospheric correction was undertaken for aerosols, which primarily affect the visible channel, because of limitations in current spatially explicit aerosol retrieval techniques. Cloud cover estimates were derived by setting a threshold (12%) on visible channel reflectance and correcting these for confusion with snow cover in early season acquisitions. A data gap between 9 June and 8 July occurred largely due to smoke from fires.

Maps of incident photosynthetically active radiation (PAR) at 1 km$^2$ spatial resolution were prepared by BOREAS collaborators [*Gu and Smith*, 1997] using Geostationary Observational Environmental Satellite (GOES) data at 30 min intervals. The instantaneous PAR maps were integrated to daily values and resampled to the AVHRR observational grid.

Maps of historical mean annual air temperature and surface spectral emissivity were the only other input data required to drive the model. Long-term mean air temperature was extracted from a map compiled by *Leemans and Cramer* [1991]. Surface emissivity was derived from a map produced by the Clouds and Earth Radiant Energy Experiment (CERES) project using field measurements reported by *Salisbury and D'Aria* [1992]. All other environmental variables were retrieved from the satellite observations alone, as described below.

## 4. Overview of the Production Efficiency Model

The PEM used in this study was a second-generation version of the global production efficiency model (GLO-PEM) [*Prince and Goward*, 1995]. GLO-PEM was developed to simulate GPP and NPP over large areas using algorithms driven entirely with remotely sensed measurements. GLO-PEM2 has an improved autotrophic respiration component, a modified temporal integration scheme, better data screening procedures, and other updates [*Goetz et al.*, 1999].

Production efficiency models are based on restrictions in the conversion "efficiency" of absorbed photosynthetically active radiation (APAR) to primary production through short-term environmental physiology. The conversion term, which we refer to as the carbon yield of APAR (ε, gC/MJ), has also been referred to as the dry matter yield of energy and, more generally, as light use efficiency [*Prince*, 1991; *Goetz and Prince*, 1996].

An advantage of the PEM approach is that consistent measurements can be made across large areas because of the contiguous nature of satellite observations without recourse to complex ecophysiological parameterization with data that are difficult or impossible to acquire at sufficiently fine resolution. Variations on the PEM approach have been used by various investigators beginning with correlative models first described by *Kumar and Monteith* [1982], *Tucker et al.* [1985], and *Asrar et al.* [1985]. In contrast, GLO-PEM2 utilizes variables retrieved entirely with remotely sensed observations and independently modifies ε in terms of both GPP ($\varepsilon_g$) and NPP ($\varepsilon_n$) without recourse to parameterizations dependent on a land cover classification.

GLO-PEM2 consists of linked models of canopy radiative transfer, canopy utilization of APAR, and physical environmental variables that reduce potential production. Potential photosynthetic rates were determined by vegetation light absorption and ambient air temperature ($T_a$) and reduced by stress terms, including vapor pressure deficit ($D$), a soil moisture cumulative stress index (CSI), and $T_a$. The "stressed" photosynthetic rates are used to provide an actual value of daily carbon assimilation, which is subsequently reduced to net carbon gain by subtraction of respiratory carbon costs.

The surface variables required to implement GLO-PEM2 were acquired using retrieval algorithms driven by the AVHRR optical and thermal measurements (Table 1). The normalized difference vegetation index (NDVI) was calculated from the infrared (IR) and visible channel (Vis) reflectance as (IR-Vis)/(IR+Vis). Brightness temperatures in channels 4 and 5 ($T_4$ and $T_5$) were calculated using calibrated radiance and applying nonlinear corrections [*Cihlar et al.*, 1997].

The biophysical surface variables can be presented as maps (Table 2). They fall into two general categories: environmental (physical) and plant (biological). The individual biological model components are briefly summarized here. More detailed description of the model is reported by *Prince and Goward* [1995] and *Goetz et al.* [1999].

The volume of data processed for the BOREAS region model runs included 1.1 Gb of input data, consisting of four spectral channels of the 1 km² AVHRR daily data, GOES PAR data at comparable spatial resolution, and other required image data (Table 1). When maps of all the output variables listed in Table 2 were generated for each of the 34 observational days, a total of 2.7 Gb data were produced. Another 1 Gb was output for those variables integrated annually, and 2 Gb of were required for intermediate image data products. Thus a total of 7 Gb storage was required for the annual (1994) model run.

### 4.1. Biological Model Components

Fractional PAR absorption ($F_{par}$) by the vegetation canopy is a key biological variable that is related to the NDVI through their joint dependence on foliage display. Whereas $F_{par}$ is known to become nonlinear in some cases because of factors other than the amount of photosynthetically active foliage (e.g., viewing geometry and background spectral properties) [*Goel and Qin*, 1994; *Goward and Huemmrich*, 1992; *Myneni et al.*, 1992], the extent of linearity (or nonlinearity) at spatial resolutions of the order of ≥1 km² has yet to be adequately addressed for heterogeneous land cover. We believe that the current quality and spatial resolution of land cover maps for the region are inadequate for type-specific $F_{par}$ models and that the problem is unresolved for mixtures of different vegetation types.

**Table 1.** GLO-PEM2 Input Variables

| Input Variable | Variable Definition | Unit of Measurement | Data Source | Data Range |
|---|---|---|---|---|
| Visible | spectral exoatmospheric reflectance | % | AVHRR channel 1 | 2, 25 |
| Near infrared | spectral exoatmospheric reflectance | % | AVHRR channel 2 | 10, 50 |
| $T_4$ | thermal emission (brightness temperature) | °C | AVHRR channel 4 | 10, 50 |
| $T_5$ | thermal emission (brightness temperature) | °C | AVHRR channel 5 | 10, 50 |
| NDVI | normalized difference vegetation index | unitless | (NIR-Vis) / (NIR+Vis) | 0.1, 0.7 |
| $T_c$ | climatological mean air temperature | °C | *Leemans and Cramer* [1991] | 5, 35 |
| Incident PAR | incident photosynthetically active radiation | MJ d$^{-1}$ | GOES, *Gu and Smith* [1997] | 5, 12 |
| $e$ | surface spectral emissivity | unitless | CERES | 0.8, 1.0 |

GLO-PEM is the global production efficiency model; AVHRR is the advanced very high resolution radiometer; NIR is near-infrared; Vis is visible channel; and CERES is the Clouds and Earth Radiant Energy Experiment. All other variables are inferred from the GLO-PEM input variables. Data ranges are for the growing season only, as defined by air temperature above 0°C and the available AVHRR imagery (April 16 to September 7 1994).

**Table 2.** GLO-PEM2 Output Variables and Image Products

| Output Variable | Variable Definition | Unit of Measurement | Data Range (min, max) |
|---|---|---|---|
| $T_s$ | surface radiometric temperature | °C | 0, 50° |
| $T_a$ | ambient air temperature | °C | 0, 50° |
| $D$ | vapor pressure deficit | millibars (mbar) | 0, 50 |
| CSI | cumulative surface wetness index | unitless | -5, 5 |
| APAR | absorbed photosynthetically active radiation | megajoules (MJ) | 0, 12 $d^{-1}$<br>100, 1100 $yr^{-1}$ |
| $W$ | standing above-ground biomass | kg $m^{-2}$ | 0, 40 |
| GPP | gross primary production | gC $m^{-1}$ | 0, 40 $d^{-1}$<br>0, 1900 $yr^{-1}$ |
| $R_a$ | autotrophic respiration | gC $m^{-1}$ | 0, 35 $day^{-1}$<br>0, 1100 $yr^{-1}$ |
| NPP | net primary production | gC $m^{-1}$ | 0, 20 $day^{-1}$<br>0, 850 $yr^{-1}$ |
| ε | carbon yield of APAR | gC $MJ^{-1}$ | 0, 1.25 |

Data ranges are for the growing season only, as defined by air temperature above 0°C and the available AVHRR imagery (April 16 to September 7 1994).

Whereas estimation of $F_{par}$ in different vegetation types, even different forest types, is a research issue beyond the scope of this paper, we modeled $F_{par}$ as a linear function of the NDVI, scaled to the range of NDVI and $F_{par}$ values observed for the region [*Chen*, 1996]. The coefficients in (1b) were fit from a range of simulations for a wide variety of viewing and solar conditions [*Goward and Huemmrich*, 1992], accounting for the effect of aerosols on the NDVI [*Tanré et al.*, 1992; *Prince and Goward*, 1995]. The range of $F_{par}$ in the simulations was comparable to that at BOREAS (0-0.8) [*Chen*, 1996]. $F_{par}$ results were compared to an independent model that used field measurements and land cover information from the BOREAS study sites [*Liu et al.*, this issue]:

$$F_{par} = (1.67)*(NDVI) - 0.08 \quad (1a)$$

(unitless). Maps of $F_{par}$ for each of the 34 image acquisition dates were combined with independently derived incident daily PAR images [*Gu and Smith*, 1997] to produce maps of canopy PAR absorption ($APAR_t$) at time t. Integration through the growing season produced an annual APAR map.

$$APAR_t = (F_{par})* (PAR_t) \quad MJ \quad (1b)$$

Potential GPP was calculated for each time interval as the product of the derived APAR maps and the potential (unstressed) carbon yield of APAR ($\varepsilon_g$* in gC $MJ^{-1}$). For C3 photosynthesis (which applies to all of the BOREAS region), $\varepsilon_g$* was a function of the ambient air temperature $T_a$, the $CO_2$ compensation point, and the $O_2/CO_2$ specificity ratio [after *Collatz et al.*, 1991; *Prince and Goward*, 1995]. We refer to this potential photosynthetic rate as quantum yield α, although we recognize the traditional use of this term as a leaf- rather than canopy-level assimilation rate relative to photon flux density. Canopy quantum yields are lower than leaf-level values because of attenuation of light through the canopy and scaling of other resources [*Field*, 1991; *Ruimy et al.*, 1995; *Goetz and Prince*, 1999]. Potential GPP was reduced by scalars that simulate stomatal control, including $T_a$, vapor pressure deficit $D$, and an index of root-zone soil moisture (CSI).

$$GPP = APAR * \varepsilon_g \quad gC\ m^{-2}\ d^{-1} \quad (2a)$$

where

$$\varepsilon_g = f(T_a, D, CSI)\ \varepsilon_g* \quad gC\ MJ^{-1} \quad (2b)$$

$$\varepsilon_g* = 55.2\ \alpha \quad (2c)$$

Derivation of the "stress" terms ($T_a$, $D$, and CSI) is discussed in section 4.2.

The loss of assimilated carbon via autotrophic respiration $R_a$ was modeled using a semiempirical relationship with standing aboveground biomass ($W$ in kg $ha^{-1}$) [*Hunt*, 1994] adjusted for the exponential response of respiration to the deviation of air temperature $T_a$ from historical, or climatological, air temperature $T_c$ [*Leemans and Cramer*, 1991]. $W$ was calculated from the minimum annual visible channel reflectance ($\rho_{min}$, %), assuming increased canopy shadowing for higher biomass canopies [*Yang and Prince*, 1997], corrected for variations in solar geometry, clouds, and cloud shadows [*Prince and Goward*, 1995].

$$R_a = \left[0.53\left(\frac{W}{W+50}\right)\right] e^{0.5\left(\frac{T_c - T_a}{25}\right)} \quad gC\ m^{-2}\ d^{-1} \quad (3a)$$

where

$$W = 7166.1\left(\rho_{min}^{-2.6}\right) \quad kgC\ ha^{-1} \quad (3b)$$

Note that lower values of $\rho_{min}$ produce higher biomass values and vice versa. The ratio of aboveground respiration to GPP is assumed to apply to the entire plant, thus we do not estimate belowground biomass. That is, the carbon costs of autotrophic respiration apply, as a proportion, to the whole plant.

NPP was calculated as the difference between total carbon assimilation (i.e., GPP) and $R_a$. As with the other environmental and biophysical variables, GPP, $R_a$, and NPP were in-

terpolated between satellite data acquisitions using time-weighted linear interpolation. Annual (growing season) results were derived from summed daily values. In terms of NPP, net carbon yield was calculated simply as the ratio of NPP to APAR ($\varepsilon_n$ in gC MJ$^{-1}$).

### 4.2. Environmental Model Components

The environmental components of GLO-PEM2 are presented here even more briefly than the biological components because their development and validation have been previously reported. Surface radiometric temperature $T_s$ was used in the calculation of several other environmental variables and biophysical variables. $T_s$ was calculated using a split-window approach [e.g., *Goetz*, 1997], which takes advantage of differential atmospheric water vapor absorption between two thermal spectral bands. The algorithm also accounts for variations in surface spectral emissivity and bandwidth differences among NOAA sensors [*Czajkowski et al.*, 1998].

A contextual approach using $T_s$ and spectral vegetation indices, known as TVX [*Goward et al.*, 1994], was used to derive spatially explicit maps of $T_a$ from ordinary least squares regression of NDVI on $T_s$. The approach assumes that $T_s$ of a fully vegetated canopy approximates $T_a$ because of the similar heat capacity of dense vegetation and the surrounding air [*Goward et al.*, 1994]. Whereas the difference between $T_s$ and $T_a$ is likely to vary with canopy aerodynamic roughness and windspeed, comparisons of $T_a$ derived using TVX have been shown to be within 2°C rms error of field measurements at a diverse range of study sites [*Czajkowski et al.*, 1997b; *Prihodko and Goward*, 1997; *Prince et al.*, 1998]. Deviations of this magnitude may result in significant errors in energy balance calculations but the effect on plant growth is relatively smaller.

An important environmental control of photosynthesis is the water vapor pressure deficit $D$, defined as the difference between saturated and actual vapor pressure. $D$ was calculated using the recovered value of $T_a$ and a dewpoint temperature $T_d$ derived from atmospheric precipitable water vapor amount $U$ extrapolated to the surface [after *Smith*, 1966]. The value of $U$, as with $T_a$, was estimated using the thermal split-window approach.

Root-zone soil moisture, referred to as a CSI, was calculated using TVX and its observed relationship with surface soil moisture [*Goetz*, 1997; *Goward et al.*, 1994; *Nemani et al.*, 1993]. A simple "bucket" model was used in which water was removed from the bucket (root volume) when slopes were steeply negative and was added to the bucket when slopes were shallow or positive [*Prince and Goward*, 1995]. The NDVI-$T_s$ slopes were normalized to a standard solar zenith angle.

The environmental variables retrieved with the various algorithms were used as surrogates for stomatal control (2b) in calculations of photosynthesis and respiration. For example, CSI was applied as a scalar (between 0 and 1), reducing potential photosynthetic rates when the TVX index of volumetric soil moisture in the root zone fell below 20%. $D$ reduced potential photosynthesis over the full range of recovered values (0 - 50 mbar).

## 5. Results

We analyzed the application of GLO-PEM2 to the BOREAS region following mapped results of the fraction of incident PAR absorbed by the vegetation canopy ($F_{par}$), GPP, total aboveground biomass, the proportion of GPP expired as autotrophic respiration, NPP, and the carbon yield of APAR. We also examined the sensitivity of modeled NPP to key driving variables. Analyses of the surface environmental variable recoveries ($T_a$, $D$, and CSI) are reported elsewhere [e.g., *Czajkowski et al.*, 1997b; *Prince et al.*, 1998].

### 5.1. Canopy Light Absorption

The fraction of PAR absorbed by the canopy ($F_{par}$) was an important variable in the PEM approach because it was used to calculate canopy APAR which drove photosynthesis. We compared GLO-PEM2 maps of $F_{par}$ with similar maps of the area derived by the Canadian Center for Remote Sensing (CCRS) [*Chen*, 1996; *Li et al.*, 1997]. The CCRS approach was based on the calibration of surface $F_{par}$ measurements to AVHRR vegetation index values stratified by 10 land cover-type classes. It also uses information on canopy structure and woody versus foliar biomass to account for PAR absorption by photosynthetic materials and for PAR reflectance from the ground surface (i.e., PAR transmitted through the canopy and reflected back again). Thus it was substantially more complex and required more information on the forest canopy and ground surface than did the linear model used in GLO-PEM2 (1b).

Comparison of GLO-PEM2 and CCRS maps across the entire BOREAS region showed $F_{par}$ values within ±0.3 in all cases (Figure 2). Actual $F_{par}$ values ranged between 0.0 and 1.0 for both models. On average the linear $F_{par}$ model produced higher $F_{par}$ values than CCRS (+0.17). Positive correlation between the two approaches based on multiple sets of independently drawn random samples ($n$=10,000) on each of three time periods (May 22-31, July 22-31, and September 1-10) was statistically significant in each case ($p<0.001$). Area-averaged differences among land cover classes (mapped by *Steyaert et al.* [1997]) ranged from a low of 0.04 for upland dense needleleaf species (i.e., primarily black spruce and jack pine) to a maximum of 0.21 for agriculture and range land (Table 3). The greatest differences between the two approaches occurred in vegetation of low canopy stature (e.g., grass and range lands, fens, tundra, and agriculture) rather than in forested areas. This result was contrary to what we expected because of the greater complexity of forest canopy structure and radiative transfer (discussed later).

When coupled with the amount of incident PAR, the $F_{par}$ term was used to produce regional canopy APAR maps for each of the 34 AVHRR acquisition dates (Plate 1a). The annual APAR values ranged from ~100 to 1100 MJ m$^{-2}$, with most values in the range 200-900 MJ m$^{-2}$. A gradient in APAR from south to north corresponded to agricultural crops and densely forested areas in the south that gradually gave way to less dense forest cover and tundra in the north.

### 5.2. Canopy Carbon Assimilation

The APAR maps, when coupled with recovered environmental variables ($T_a$, $D$, and CSI), provided maps of canopy carbon assimilation (i.e., GPP) (Plate 1b). GPP values ranged from 0 to 1900 g C m$^{-2}$ yr$^{-1}$, with most values in the range 0-1500 g C m$^{-2}$ yr$^{-1}$. Spatial patterns of GPP were related to land cover types with the highest values associated with patches of broadleaf forest in the southeastern portion of the region and the lowest values associated with tundra in the north and ag-


**Figure 2.** A difference image of two independently derived $F_{par}$ maps for the time period July 22-31, 1994. The six Advanced Very High Resolution Radiometer (AVHRR) scenes available for the 10 day period, each of which were used in the production efficiency model (PEM) to calculate $F_{par}$, were composited using the maximum normalized difference vegetation index (NDVI) technique [*Holben*, 1985] for comparison with the $F_{par}$ approach used in the Canadian Center for Remote Sensing (CCRS) model. Light tones indicate where the PEM exceeded CCRS $F_{par}$, and dark tones indicate the opposite. Lakes appear white.

riculture in the south. The agricultural areas had low productivity compared with natural vegetation because of periods of bare ground and reduced cover between crops.

Comparisons with canopy carbon assimilation estimates, provided by eddy covariance flux measurements [e.g., *Baldocchi and Vogel*, 1996; *Black et al.*, 1996; *Goulden et al.*, 1997] highlighted differences in the two approaches (Figures 3a-3c). In the examples shown few satellite acquisitions were available early or late in the growing season when conditions (e.g., foliar phenology) were rapidly changing. The lack of early season (April and May) acquisitions at many measurement sites was primarily a result of cloud cover obscuring large portions of the land surface at the time. The midseason data gap was primarily a result of smoke and haze from major forest fires (1994 was one of the more active fire years on record).

Despite the temporal data gaps in the satellite record the magnitude of GPP values estimated by eddy covariance and modeled with GLO-PEM2 were comparable. The aspen site (Figure 3a) had the greatest flux magnitude of the seven sites equipped for such measurements, exceeding 170 kg C $ha^{-1}$ $d^{-1}$. In contrast, the spruce (Figure 3b) sites did not exceed 90 kg C $ha^{-1}$ $d^{-1}$, and pine sites (Figure 3c) peaked at just over 60 kg C $ha^{-1}$ $d^{-1}$. Substantial divergence of the measured and modeled values were observed, particularly in the southern old jack pine (S-OJP) site, but the temporal evolution of GPP throughout the growing season was reasonably well charac-

**Table 3.** The Difference Between GLO-PEM2 and CCRS $F_{par}$ ($\Delta F_{par}$), the Dry Matter Yield of APAR in Terms of Net Production $\varepsilon_n$ and Gross Production $\varepsilon_g$, and the Proportion of GPP (Canopy Assimilation) Lost to Autotrophic Respiration ($R:A$ ratio) for the BOREAS Region

| Landcover Type Class | $\Delta F_{par}$ | $\varepsilon_n$, g C MJ$^{-1}$ | $\varepsilon_g$, g C MJ$^{-1}$ | $R:A$ |
|---|---|---|---|---|
| Lowland needleleaf (sparse) | 0.10 | 0.49 | 1.19 | 0.53 |
| Regeneration (mostly needleleaf) | 0.12 | 0.45 | 1.25 | 0.56 |
| Agriculture, pasture | 0.21 | 0.43 | 1.03 | 0.53 |
| Mixed forest (needleleaf, broadleaf) | 0.11 | 0.62 | 1.39 | 0.59 |
| Mixed forest (mostly broadleaf) | 0.08 | 0.62 | 1.64 | 0.61 |
| Mixed forest (mostly needleleaf) | 0.08 | 0.47 | 1.26 | 0.60 |
| Lowland needleleaf (dense) | 0.07 | 0.46 | 1.31 | 0.62 |
| Sparsely vegetated | 0.18 | 0.42 | 1.16 | 0.52 |
| Upland needleleaf | 0.04 | 0.43 | 1.24 | 0.50 |
| Regeneration (mostly broadleaf) | 0.06 | 0.55 | 1.50 | 0.58 |
| Recently burned | 0.26 | 0.38 | 1.05 | 0.49 |
| Grasses, marsh | 0.20 | 0.45 | 1.23 | 0.46 |

CCRS, Canadian Center for Remote Sensing; BOREAS, Boreal Ecosystem-Atmosphere Study. Data were categorized by land cover type as mapped by *Steyaert et al.* [1997].

terized by GLO-PEM2 for those sites exhibiting clear phenological changes in GPP.

Because the satellite observations have a nominal spatial resolution > 1 km$^2$, it was difficult to assess the absolute accuracy of the GPP results. Nevertheless, we also compared GLO-PEM2 with independent measures of carbon exchange as derived from a combination of tree ring increment measurements and model simulation [*Gower et al.*, 1997; *Ryan et al.*, 1997]. The GPP values were similar despite the differences in modeling, measurement techniques, and spatial scales (Table 4). GLO-PEM2 GPP at the five sites where data were available agreed with the surface measurements to within 30% in all cases, ranging from an underestimate of 30% for the southern old black spruce (S-OBS) to an overestimation of 16% for the S-OJP.

### 5.3. Aboveground Biomass

Spatial patterns in the GLO-PEM2 above-ground biomass map (Plate 1c) captured the large contrast between agricultural areas (in the southwest), dense boreal forest (occupying a strip from the southeast to northwest), and tundra (in the northeast, approaching Hudson Bay). The isolated patches of broadleaf forest noted in the GPP image were also clearly delineated (in the southeastern portion of the region). The aboveground biomass values ranged between 0 and 40 kg m$^{-2}$, with most values in the range 0-30 kg m$^{-2}$.

The biomass map was compared with the estimates made with two independent remotely sensed techniques as well as field measurements of biomass at study plots (five 5 m$^2$ plots within a 30 m$^2$ radius) [*Gower et al.*, 1997]. None of the methods other than GLO-PEM2 mapped the entire BOREAS region, so spatial comparisons were limited to a 420 km$^2$ region common to all the biomass mapping techniques. The first of these used a mixture model of multispectral Landsat Thematic Mapper observations [*Hall et al.*, 1997]. The other was a semiempirical technique using C-band Shuttle Imaging Radar (SIR-C) data in which the biomass recoveries were calibrated with field biomass estimates [*Ranson et al.*, 1997]. The biomass maps produced with these various techniques were resampled (using bicubic convolution) from their original 30 m$^2$ resolution to 1 km$^2$ spatial resolution for comparison with GLO-PEM2 biomass. We note that the mixture-model biomass was based on a single thematic mapper (TM) scene (September 2) and the SIR-C biomass was derived for a single acquisition (October 6).

Spatial comparisons of the biomass maps were reported by *Johnston* [1998]. All the biomass maps had the same magnitude of error relative to the field biomass estimates (rms errors were 4.5-5.9 kg m$^{-2}$ for a range of 15.8 kg m$^{-2}$, $n$=16). The TM mixture model had the lowest rms error, and GLO-PEM2 had the highest. The GLO-PEM2 biomass also overestimated the field values (+4.2 kg m$^{-2}$). To compensate for this bias, the biomass map was, as with the SIR-C map, calibrated to the field biomass estimates. This avoided compounding errors in the calculation of autotrophic respiration (reported in the section 5.4).

There was no observed trend in biomass estimation error between forest cover types (i.e., areas dominated by spruce, pine, or aspen). It was not possible to assess absolute error in other types of land cover (e.g., in tundra, pasture, etc.) because field measurements were limited to forested areas. An assessment of errors introduced by spectral mixing of land cover types was possible, however, by calculating the proportion of cover types within each 1 km$^2$ cell using the full resolution TM map. This analysis suggested that 15% of the error in the GLO-PEM2 biomass estimates (relative to the TM mixture model) were a result of cover-type mixing within the 1 km$^2$ cells. The greatest differences between the GLO-PEM2 and TM mixture model results were, as with the errors in $F_{par}$, primarily restricted to areas of low-stature vegetation (fen and regenerating forests). These were areas where background reflectance and surface water most strongly affect the recovery technique.

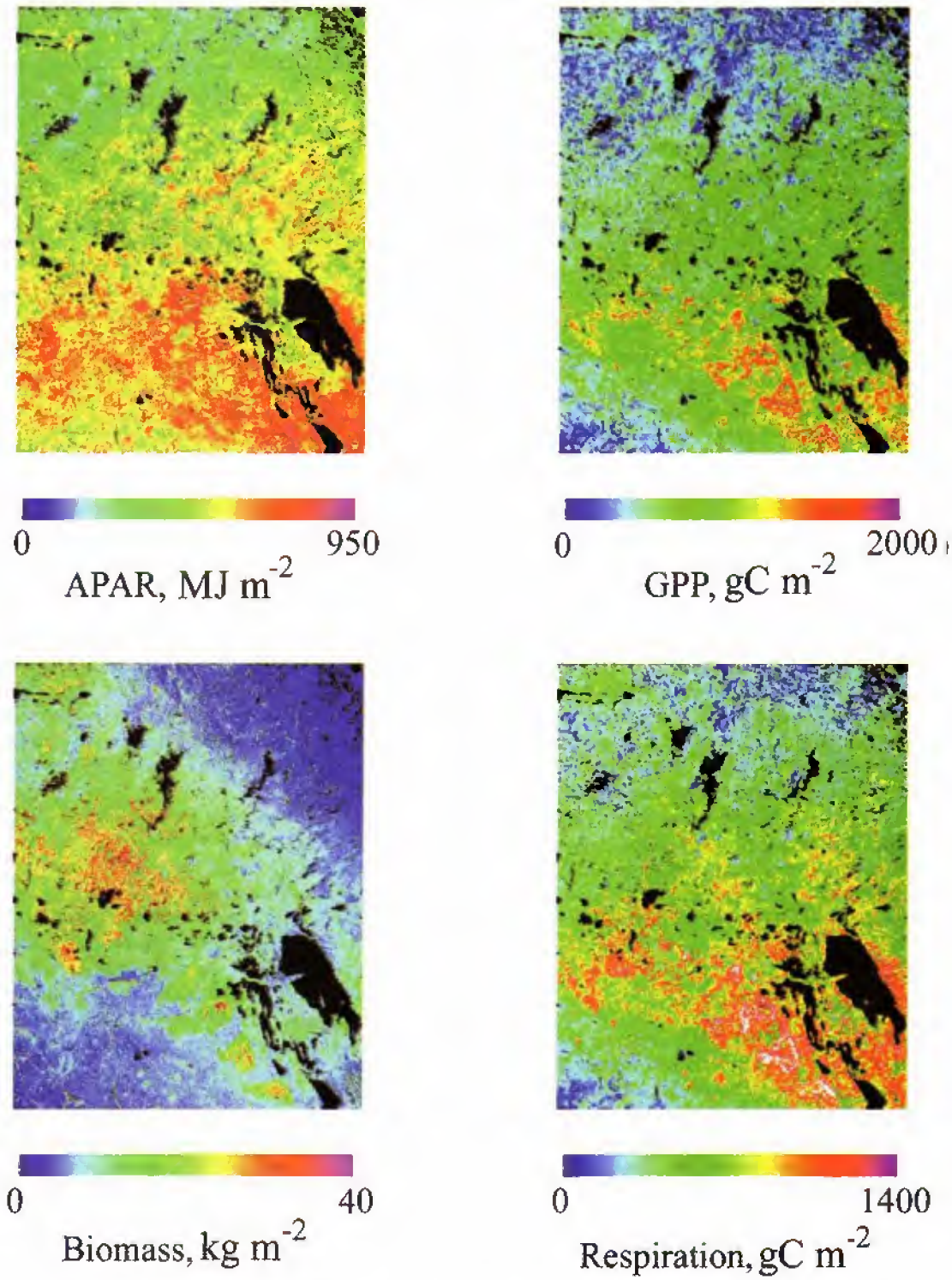


**Plate 1.** Maps of variables derived from the PEM for the year 1994. The images cover an 800 by 1000 km portion of the BOREAS study region, oriented with north at the top; lakes appear black (Lake Winnipeg is the largest of these, in the southeast portion of the image): (a) absorbed photosynthetically active radiation (APAR), (b) gross primary production (GPP), (c) standing aboveground biomass, and (d) autotrophic (plant) respiration.

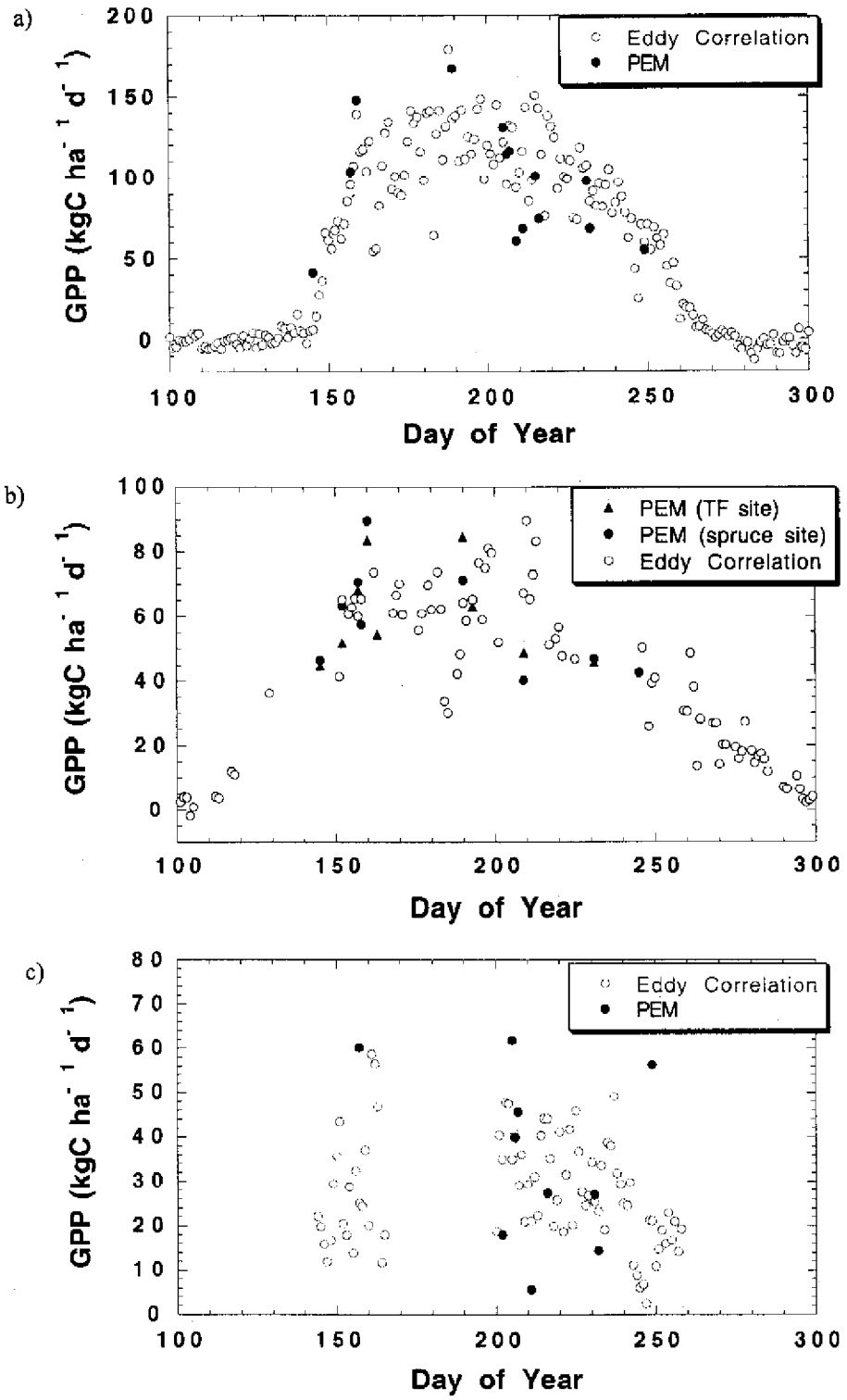


**Figure 3.** Daily carbon uptake (GPP) as measured from tower site eddy covariance versus the PEM: (a) southern old aspen (S-OA) site, (b) northern black spruce (N-OBS) site, and (c) southern old jack pine (S-OJP) site.

### 5.4. Canopy Autotrophic Respiration

The GLO-PEM2 autotrophic respiration image (Plate 1d) showed spatial patterns similar to GPP, reflecting the high correlation of these variables. $R_a$ values ranged from 0 to 1100 g C $m^{-2}$ $yr^{-1}$, but most values fell in the range 0-900 g C $m^{-2}$ $yr^{-1}$. The proportion of GPP lost to respiration (the $R_a$:GPP or $R$:$A$ ratio) was variable across the BOREAS region because of differences in air temperature, land cover type, and biomass. The $R$:$A$ ratio ranged between 0.45 and 0.75, with most values in the range 0.52-0.70 and a mean of 0.61. The coefficient of variation (cv) in the $R$:$A$ ratio was 9.35%. Biomass alone accounted for 67% of the variability in the $R$:$A$ ratio ($n$=25).

**Table 4.** GLO-PEM2 Values for GPP, Total NPP, $R_a$, and the Ratio of Respiration to GPP (i.e., Assimilation $A$) ($R_a/A$)

| Variable | N-OBS | N-OJP | N-YJP | S-OBS | S-OJP | S-YJP | S-OA |
|---|---|---|---|---|---|---|---|
| $n$ | 9 | 11 | 6 | 14 | 10 | 16 | 14 |
| | | | | *PEM* | | | |
| GPP | 1040 | 720 | 1029 | 759 | 899 | 949 | 1206 |
| $R_a$ | 638 | 437 | 601 | 477 | 577 | 562 | 758 |
| NPP | 402 | 284 | 429 | 282 | 322 | 387 | 448 |
| $R_a/A$ | 0.61 | 0.61 | 0.58 | 0.63 | 0.64 | 0.59 | 0.63 |
| | | | | *Field* | | | |
| GPP | 1080 | 880 | NA | 1090 | 772 | NA | 1350 |
| $R_a$ | 828 | 651 | NA | 783 | 535 | NA | 910 |
| NPP | 252 | 229 | NA | 307 | 237 | NA | 440 |
| $R_a/A$ | 0.77 | 0.74 | NA | 0.72 | 0.69 | NA | 0.67 |
| | | | | *Difference %* | | | |
| GPP | -4 | -18 | NA | -30 | 16 | NA | -11 |
| $R_a$ | -23 | -33 | NA | -39 | 8 | NA | -17 |
| NPP | 60 | 24 | NA | -8 | 36 | NA | 2 |
| $R_a/A$ | -20 | -18 | NA | -12 | -7 | NA | -7 |

The number of samples (images) available for annual integration are indicated as $n$. The difference between field estimates of these same variables [*Ryan et al.*, 1997] and PEM values are given. Field sites include, for the northern (N) and southern (S) study areas, old jack pine (N-OJP, S-OJP), young jack pine (N-YJP and S-YJP), old black spruce (N-OBS and S-OBS) and old aspen (S-OA).

Most of the remaining variation (15%) was accounted for by the carbon yield of APAR. Areas of high biomass, high GPP, and relatively high ambient air temperature during the growing season had the greatest respiratory fluxes (e.g., the isolated patches of broadleaf forest in the southeastern portion of the image).

It was not possible to compare directly the GLO-PEM2 respiration values with flux measurements because autotrophic and heterotrophic fluxes within the eddy covariance measurements are not separated, specifically because belowground respiratory fluxes were inseparable with current isotopic tracer tagging techniques. We did, however, compare the GLO-PEM2 respiration values with those calculated by semiempirical models driven with field measurements [*Lavigne and Ryan*, 1997; *Ryan et al.*, 1997].

The GLO-PEM2 canopy respiration values tended to underestimate relative to those derived from the combination of measurements and modeling (Table 4). The greatest underestimation was for the S-OBS site (39%), and the largest overestimation was for the S-OJP site (8%). In terms of the proportion of GPP lost to respiration (the $R$:$A$ ratio), GLO-PEM2 values also tended to be lower than the measurement-based estimates, with differences ranging from −20% (N-OBS) to +7% (S-OJP). The changes between sites in the comparison of measured and modeled values reflect "errors" in the $R$:$A$ values brought about by the incorporation of both the GPP and $R_a$ terms. The observed errors in GPP and $R_a$ never occurred in opposite directions, thus sites where GPP was overestimated relative to field values were also those sites where $R_a$ was overestimated. This suggests that there was some offsetting of errors in the $R$:$A$ comparisons and in the derived maps of NPP (i.e., the difference between GPP and $R_a$).

### 5.5. Net Primary Production and Regional Carbon Uptake

Only 35% of the variability in NPP was explained by the annual sum of the NDVI, thus the NPP map was not a simple transform of the satellite vegetation index maps. The remaining variability in NPP within the region was driven by a combination of light harvesting (i.e., APAR), the suite of environmental variables that affect light use, and differences in respiration relative to GPP resulting from variations in biomass and temperature. The order of these differed temporally and with vegetation type [*Thawley*, 1998] (see later discussion). We found the two variables that had the strongest effect on the value of NPP estimated with GLO-PEM2, as determined by their relative contribution calculated from an analysis of variance, were vapor pressure deficit $D$ and APAR. These variables were not independent, however, but showed a strong interaction owing to high correlation in each of the three dominant forest canopy species.

The GLO-PEM2 map of total annual NPP (Plate 2) ranged from 0 to 850 g C $m^{-2}$ $yr^{-1}$, but the great majority of values were within the range 0-600 g C $m^{-2}$ $yr^{-1}$. The spatial pattern of NPP was comparable to those for GPP and $R_a$, with higher values in the forest areas compared to tundra and agriculture. High biomass values in the west central portion of the region tended to reduce NPP in those regions because of greater respiratory cost estimates. Similar patterns and magnitudes of NPP were reported by *Liu et al.* [this issue].

NPP values derived from GLO-PEM2 at the field sites fell within a smaller range (~200-500 g C $m^{-2}$ $yr^{-1}$) than for the entire BOREAS region. This reduced range was comparable to the field estimates of NPP (Table 4). The difference between the two was as little as 2% (S-OA) and as great as 60% (N-OBS), with an average overestimation of 23% for these five sites (the only field sites where full carbon budgets were available) [*Gower et al.*, 1997; *Ryan et al.*, 1997]. Additional field NPP measurements were available at "auxiliary" sites located throughout the BOREAS region; however, despite an effort to locate these additional sites in stands representative of a larger area surrounding the plots [*Apps and Halliwell*, 1994], the extreme spatial heterogeneity of the boreal landscape made it impossible to use them for comparison with observations at the 1 $km^2$ spatial scale. Compared to the field sites where full carbon budgets were available and the two estimates of NPP were positively and significantly related

**Table 5.** The Proportion of Each Land Cover Type and PEM-Derived Values of Average NPP and Total Carbon Uptake for the BOREAS Region, Categorized by Land Cover Type

| | Regional Uptake Tg C | NPP gC $m^{-2}$ $yr^{-1}$ | Proportion of Area, % |
|---|---|---|---|
| Lowland needleleaf (sparse) | 33.1 | 288 | 18.0 |
| Regeneration (mostly needleleaf) | 22.7 | 296 | 12.0 |
| Agriculture, pasture | 17.8 | 338 | 8.2 |
| Mixed forest (needle / broadleaf) | 17.7 | 342 | 8.1 |
| Mixed forest (mostly broadleaf) | 15.8 | 448 | 5.5 |
| Mixed forest (mostly needleleaf) | 13.5 | 285 | 7.4 |
| Lowland needleleaf (dense) | 13.2 | 296 | 7.0 |
| Sparsely vegetated | 10.4 | 282 | 5.8 |
| Upland needleleaf | 10.3 | 355 | 4.5 |
| Regeneration (mostly broadleaf) | 7.30 | 392 | 2.9 |
| Recently burned | 6.40 | 242 | 4.1 |
| Unknown | 6.08 | 273 | 3.5 |
| Grasses, marsh | 1.07 | 293 | 0.6 |
| Water | - - - | - - - | 12.4 |
| Sum uptake, area; mean NPP | 175 | 318 | 100 |

Land cover type as mapped by *Steyaert et al.* [1997].

($r^2$=0.43 and $p$<0.05), there was essentially no relationship between GLO-PEM2 and auxiliary site NPP ($r^2$=0.06). We note that the carbon budget sites were selected to be where flux towers were located, and these, in turn, were specifically selected to be in uniform vegetation cover.

Although GLO-PEM2 does not use land cover maps, NPP was quite different between land cover types across the region and was ordered in a sequence where broadleaf forest (primarily aspen and birch species) had the highest average NPP of any cover type, followed by broadleaf regeneration, upland needleleaf forest, and a mixture of deciduous and needleleaf forest. The lowest NPP values were for recently burned, "unknown," and sparsely vegetated areas. Various classes of lowland needleleaf forest including fens, bogs, and sparse cover commonly known as muskeg (dominated by black spruce and larch) were also in the lower range of NPP values.

Regional estimates of total carbon sequestration were made by incorporating the average NPP and area occupied by each land cover type (Table 5). Total carbon uptake in NPP amounted to 175 teragrams (Tg), which was, again, similar to *Liu et al.* [this issue]. Note that despite a relatively low production rate, lowland needleleaf areas sequestered the greatest amount of carbon annually because of their large areal extent. Together with needleleaf regeneration these areas accounted for nearly one third of the total regional carbon uptake. Although broadleaf forest and regeneration were characterized by high production rates, these areas accounted for just 13% of the total C uptake. Agriculture and pasture areas accounted for just over 10% of the total.

### 5.6. Carbon Yield of APAR

Values of the carbon yield of APAR (i.e., the amount of total production per unit energy $\varepsilon_n$) ranged from near 0 to 1.25 g C $MJ^{-1}$. The average value of $\varepsilon_n$ for the entire region (excluding lakes, $n$=768,428) was 0.48 g C $MJ^{-1}$. The highest values of $\varepsilon_n$ were associated with the broadleaf forest stands, and the lowest values were associated with areas of sparse vegetation cover in agricultural fields or tundra. There was less variation of $\varepsilon_n$ with land cover type (cv=39.4%) than in GPP, biomass, respiration, or NPP. Variation in NPP with APAR at a combination of flux tower and auxiliary sites of relatively homogenous vegetation cover (Figure 4) showed aspen sites had a steeper NPP/APAR slope (and corresponding $\varepsilon_n$ value of 1.11 g C $MJ^{-1}$) than did the pine sites (0.84 g C $MJ^{-1}$), and these, in turn, were greater than for the spruce (0.79 g C $MJ^{-1}$) or fen (0.65 g C $MJ^{-1}$) sites. The suite of sites was confined to a limited set merely for the purpose of referencing known locations. Values of $\varepsilon_n$ for the entire region mapped with GLO-PEM2 showed a similar order, albeit a somewhat diminished range owing to spatial averaging by land cover type (Table 3). As noted earlier, the *R:A* ratio was inversely related to and accounted for 15% of the variation in $\varepsilon_n$ ($p < 0.001$).

Carbon yield of APAR in terms of annual gross production ($\varepsilon_g$) ranged between 0 and 3.0 g C $MJ^{-1}$ for the entire BOREAS region, averaging 1.24 g C $MJ^{-1}$, and was similar to $\varepsilon_n$ in its spatial distribution and rank order by land cover class (Table 3). The variability of $\varepsilon_g$ (cv = 35.6%) was slightly less than for $\varepsilon_n$, but the difference was significant ($p < 0.001$).

## 6. Discussion

GPP values derived with GLO-PEM2 were consistent with what was expected for the various land cover types present in the study area, with a gradient ranging from the highest values in broadleaf forests to the lowest values in fens and sparsely vegetated areas. The modeled GPP values were in the same range as those estimated with eddy covariance [*Baldocchi and Vogel*, 1996; *Black et al.*, 1996; *Goulden et al.*, 1997] and from a combination of tree ring increment, chamber measurements, and fitted stand-level models [*Gower et al.*, 1997; *Lavigne and Ryan*, 1997; *Ryan et al.*, 1997]. They were also

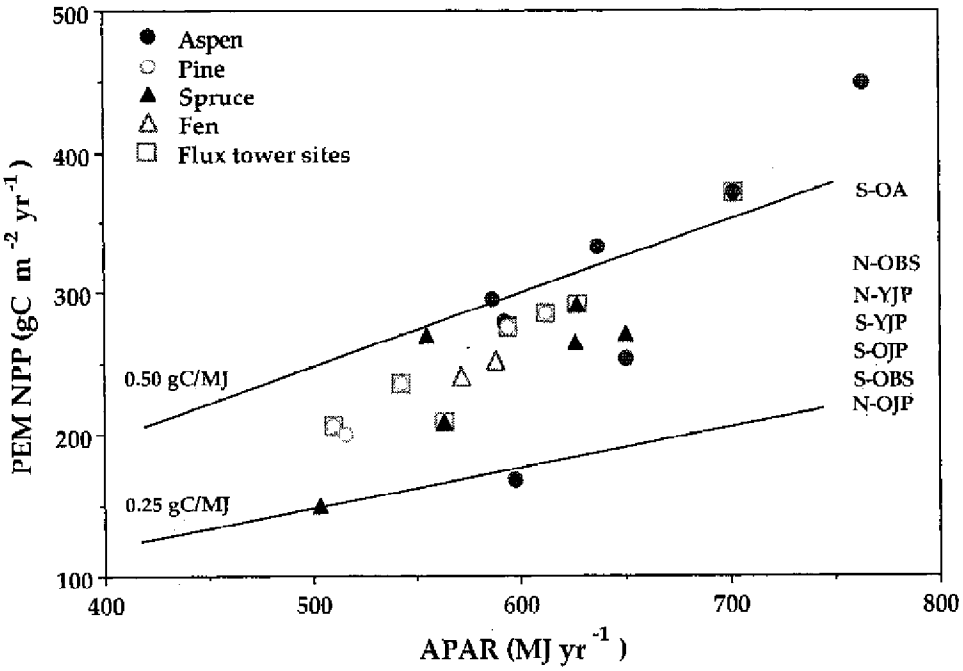


**Figure 4.** The relationship between canopy APAR and total annual NPP for a suite of flux tower and auxiliary sites of relatively homogenous vegetation cover. The lines indicate carbon yield of APAR values of 0.25 and 0.50 gC $MJ^{-1}$.

in the range of independent simulation model results conducted for the flux tower sites [*Kimball et al.*, 1997].

While providing an inherent spatial monitoring capability, GLO-PEM2 was limited in its temporal resolution because of the reduced availability and quality of satellite imagery (e.g., because of cloud cover and smoke from forest fires). The temporal limitation of satellite observations does not apply solely to GLO-PEM2, of course, but to any ecosystem model driven with satellite or other intermittent observations. Those models that use satellite data simply to initialize state variables, e.g., leaf area index (LAI), must also interpolate foliar phenological dynamics throughout the growing season. In contrast, eddy covariance techniques cannot directly provide GPP maps but do permit nearly continuous temporal measurements at a point representing variable fetch (a function of wind speed, direction, and the height of the instruments above the canopy).

The fraction of incident PAR absorbed by the vegetation canopy ($F_{par}$) was an important variable in the determination of GPP rates because, when combined with incident PAR, it provided the energy (APAR) to drive photosynthesis. Comparison of GLO-PEM2 $F_{par}$ maps with an independent model [*Lui et al.*, this issue] showed the greatest differences occurred not in forested areas but in predominantly nonwoody vegetation cover (i.e., tundra, grasslands, and agricultural areas). Other than differences between the two modeling approaches, differences in the $F_{par}$ maps may have been due to inconsistencies in the image data sets used for the two approaches. The CCRS results were derived from 10 day maximum NDVI composites of AVHRR observations [*Holben*, 1985], which required that we also composite the AVHRR data for the $F_{par}$ comparisons. For example, six AVHRR scenes were acquired during the 10 day period July 21-30, 1994 (shown in Figure 2). Nevertheless, we found very similar results for comparisons conducted with 10 day composites containing fewer AVHRR acquisitions (e.g., three acquisitions between September 1 and 10, and a single acquisition between May 22-31). These comparisons suggest that differences between the two approaches were not a result of the compositing process or other data manipulation. Rather, they were more likely a result of the effect of background (ground cover) reflectance in areas where the two models differed most and the effect of the CCRS vegetation type-specific $F_{par}$ models versus our more general model.

The autotrophic respiration ($R_a$) values modeled with GLO-PEM2 were, as with GPP, in the range of measurements at the study sites [*Lavigne and Ryan*, 1997; *Ryan et al.*, 1997]. Respiration was closely related to biomass, which was mapped with a comparable degree of accuracy as other independent techniques based on Landsat and SIR-C observations [*Hall et al.*, 1997; *Ranson et al.*, 1997]. The reason for a positive bias in the GLO-PEM2 biomass values was not resolved but may have been due to a tendency for the minimized visible reflectance technique to select image values acquired at low sun angles (~40% of the minimum visible reflectance value were from satellite acquisitions after day 215, i.e., August 3). After the positive bias in the GLO-PEM2 biomass estimation was removed by calibration with surface measurements we produced a biomass map that covered the entire BOREAS region.

Derivation of an accurate biomass map allowed us to examine proportional respiration costs relative to GPP (i.e., the *R:A* ratio). We found a range in the *R:A* ratio among cover types that was in the same range as stand-level measurements conducted at BOREAS [*Ryan et al.*, 1997] as well as empirically derived and modeled values at other boreal forest sites [*Goetz and Prince*, 1996; *Goetz and Prince*, 1998]. This result was evident despite differences in the spatial scale of the

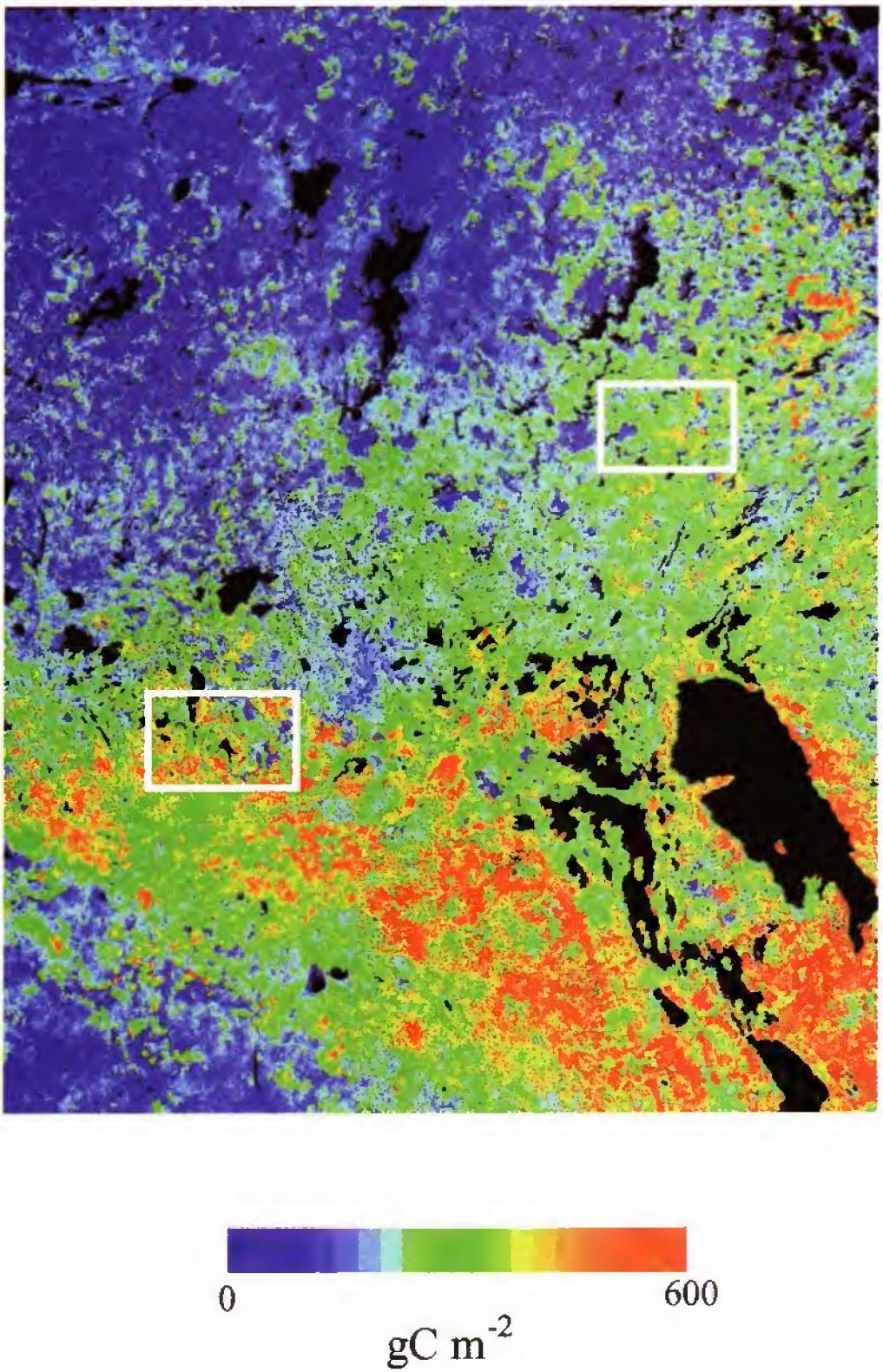


**Plate 2.** Map of total 1994 net primary production (NPP) derived from GLO-PEM2 (global production efficiency model) for the BOREAS region (see Plate 1 legend for area description). The white boxes indicate the BOREAS southern and northern study areas.

observations, i.e., spatial averaging and the associated spectral mixing of land cover components. There have been suggestions of a narrow range in the *R:A* ratio [*Gifford*, 1994; *Landsberg and Waring*, 1997; *Waring et al.*, 1998], but the current results, as well as previous analyses, suggest that the amount of GPP lost to respiration ranges between at least 45 and 75% in boreal ecosystems alone.

In terms of net primary production (i.e., the difference between GPP and $R_a$) we again found a logical progression of rates between land cover types: broadleaf deciduous stands were most productive, and an array of sparsely vegetated areas were least productive. The regulation of NPP rates was set by a combination of factors that affected GPP and $R_a$. These included, most significantly, the amount of canopy APAR and the atmospheric vapor pressure deficit *D*, the two of which covaried throughout the growing season. The dominance of these terms in determining photosynthetic rates was in agreement with leaf- and canopy-level measurements at the BOREAS sites [e.g., *Dang et al.*, 1997; *Saugier et al.*, 1997]

The range of modeled carbon yield of APAR values was comparable to measurements surveyed for other boreal and temperate forest sites [*Ruimy et al.*, 1994; *Goetz and Prince*, 1996; *Landsberg et al.*, 1997]. Empirically derived values of $\varepsilon_n$ for aboveground production of boreal forest stands in northern Minnesota, for example, ranged from 0.08 to 0.65 g C $MJ^{-1}$ [*Goetz and Prince*, 1996] and showed a similar divergence between broadleaf and needleleaf vegetation cover. Independently estimated values of $\varepsilon_n$ simulated with an ecophysiology model [*Goetz and Prince*, 1998] were within 15% of the empirical values. The order of $\varepsilon_n$ for the various cover types in the BOREAS region followed a sequence (aspen, pine, spruce, and fen) that was expected from both measured and simulated growth and productivity rates. The order of $\varepsilon_n$ at the regional scale was similar despite a reduced range of values introduced as a result of spatial averaging by land cover type.

There has been some suggestion that $\varepsilon_n$ should remain relatively invariant among different "functional types" of plants [*Field*, 1991], which would simplify the estimation of NPP with APAR alone. Recent analyses, however, suggest that convergence in $\varepsilon_n$ is not only infrequently observed but unlikely to occur primarily because of variability in the respiratory costs of production associated with different plant types, i.e., the *R:A* ratio [*Goetz and Prince*, 1999]. As noted earlier, there is conflicting information on the possible convergence of respiratory costs as a proportion of GPP, but we found a substantial range of both *R:A* values (0.45-0.75) and $\varepsilon_n$ values (0 - 1.25 g C $MJ^{-1}$). Previous work has also suggested possible convergence in gross (rather than net) production per unit energy (i.e., in $\varepsilon_g$ rather than $\varepsilon_n$) [*Goetz and Prince*, 1998]. Results of the current study showed less difference in the coefficients of variation for $\varepsilon_g$ and $\varepsilon_n$ than was observed at the stand level at the Minnesota sites, but the differences at BOREAS were also statistically significant. We attribute somewhat greater convergence in $\varepsilon_g$ than $\varepsilon_n$ to variation in $\varepsilon_n$ introduced by differences in canopy respiration relative to GPP (the *R:A* ratio). That is, those areas or cover types with relatively high respiration (as a proportion of GPP) had lower NPP relative to APAR (i.e., $\varepsilon_n$). Other areas were the reverse, resulting in variability in $\varepsilon_n$ [see also *Goetz and Prince*, 1999].

Various studies have reached different conclusions on the range of variability in the *R:A* ratio and carbon yields of APAR among different types of plants [*Goetz and Prince*, 1998; *Landsberg and Waring*, 1997; *Ruimy et al.*, 1996; *Ryan et al.*, 1997; *Waring et al.*, 1998]. These differences in the range of *R:A*, $\varepsilon_n$, and $\varepsilon_g$ may be due to a number of different factors, including differences between study areas, methodologies, vegetation types, and the scale of observation. Differences in the spatial resolution of observations and the associated mixing of plant types within any given sample will clearly have an impact on comparison studies. We must also consider the possibility that GLO-PEM2 was not sufficiently accurate in its determination of photosynthetic and respiration rates to account for all of the ecophysiological complexity of these forest stands, particularly in terms of the environmental variables that affect stomatal control. Nevertheless, GLO-PEM2 photosynthetic and respiration rates were comparable to rates measured by a suite of independent techniques at the stand level. Moreover, estimates of $\varepsilon_g$ recently derived from eddy flux estimates, measured incident PAR, and estimated NDVI-$F_{par}$ relationships [*Huemmrich et al.*, this issue] for three BOREAS sites (NSA-Fen, SSA-OBS, and SSA-OA) compared favorably with our modeled estimates of $\varepsilon_g$. The estimates based on the stand-level measurements (0.49, 0.87, and 1.39 gC $MJ^{-1}$, respectively) (K. Huemmrich, personal communication, 1999) were comparable to our modeled values for these same sites (0.31, 1.02, and 1.64 gC $MJ^{-1}$). This comparison was particularly favorable considering the intricacies of flux component separation and that the model estimates were for a >1 $km^2$ area that was relatively fixed compared to the variable fetch at the tower flux sites.

Additional work is clearly needed to establish the variability of carbon yields of APAR and the *R:A* ratio as well as their relationship to one another (particularly between *R:A* and $\varepsilon_n$) at additional study sites and at comparable scales of observation. We cannot, in any case, assume that variation in any of the terms critical to macroscale monitoring of carbon exchange will be confined to a sufficiently narrow range of values to allow for their omission from ecosystem models driven with remote sensing.

## 7. Conclusions

Maps of surface biophysical variables derived from the second-generation global production efficiency model (GLO-PEM2) captured gradients of net and gross primary production (NPP and GPP), canopy absorbed photosynthetically active radiation (APAR), aboveground biomass, canopy respiration, and carbon yields of APAR (i.e., net and gross production per unit energy) across the $10^6$ $km^2$ BOREAS region. Maps of these variables provide an important link for scaling stand-level measurements (e.g., field biomass increment measurements and $CO_2$ fluxes using eddy covariance) to larger areas and ultimately improving global models of biospheric process and function.

The GLO-PEM2 results were in good agreement with a combination of surface measurements and independent model results available for study sites within the BOREAS region. There were also clear associations of the various process rates with land cover type (i.e., broadleaf deciduous, needleleaf evergreen, etc.) despite the fact that GLO-PEM2 does not utilize land cover maps. Thus the model complements a spectrum of carbon exchange models that currently range from complex mechanistic models based on plant ecophysiology to those that rely on relatively simple bioclimatological relationships.

This first application of GLO-PEM2 at 1 km² spatial resolution supported earlier studies that suggest a somewhat greater convergence in gross carbon yield per unit APAR ($\varepsilon_g$) than the comparable value in terms of net production ($\varepsilon_n$) among different vegetation or land cover types. This is an important consideration for modeling NPP over large areas because it facilitates the use of remotely sensed observations for estimating photosynthetic rates. The results do not, however, support suggestions of convergence in either the *R:A* ratio or APAR utilization terms sufficiently to allow their omission from or overgeneralization in NPP models. This conclusion derived from the independent treatment of the respiratory and photosynthetic components of GLO-PEM2, which resulted in the balance of these (i.e., the proportion of GPP lost to canopy respiration) varying over a substantial range (45-75%).

On the basis of these observations in the BOREAS region (and previous work in other study sites) we caution against attempts to infer directly NPP using remotely sensed spectral vegetation indices without consideration of the factors that account for variability in the carbon yield of APAR and respiratory costs in relation to NPP. The production efficiency model formulation provides a methodology to account for these terms, thus an ability to monitor canopy carbon exchange and net primary production over large areas.

**Acknowledgments.** We thank our fellow BOREAS investigators for sharing their data, Charlie Shive for help with graphics, Megan Weiner for copy editting, and the reviewers for their thoughtful and thorough critiques. This work was supported by a NASA Terrestrial Ecology Program grant NAGW5178.

## References

Apps, M., and D. Halliwell, Biometry and auxiliary site locations and descriptions, report, 68 pp., Can. For. Ser., 1994. (Available at http://boreas.gsfc.nasa.gov/boreas_home)

Asrar, G., E. T. Kanemasu, R. D. Jackson, and P. J. Pinter, Estimation of total above ground phytomass production using remotely sensed data, *Remote Sens. Environ., 17*, 211-220, 1985.

Baldocchi, D. D., and C. A. Vogel, Energy and $CO_2$ flux densities above and below a temperate broad-leaved forest and a boreal pine forest, *Tree Physiol., 16*, 5-16, 1996.

Black, T. A., et al., Annual cycles of water vapour and carbon dioxide fluxes in and above a boreal aspen forest, *Global Change Biol., 2*, 219-229, 1996.

Bonan, G. B., K. J. Davis, D. Baldocchi, D. Fitzjarrald, and H. Neumann, Comparison of the NCAR LSM1 land surface model with BOREAS aspen and jack pine tower fluxes, *J. Geophy. Res., 102*, 29,065-29,076, 1997.

Chen, J., Canopy architecture and remote sensing of the fraction of photosynthetically active radiation absorbed by boreal forest conifers, *IEEE Trans. Geosci. and Remote Sens., 34*, 1353-1368, 1996.

Ciais, P., P. P. Tans, M. Trolier, J. W. C. White, and R. J. Francey, A large Northern Hemisphere terrestrial $CO_2$ sink indicated by the $^{13}C/^{12}C$ ratio of atmospheric $CO_2$, *Science, 269*, 1098-1101, 1995.

Cihlar, J., H. Ly, and F. Huang, Multitemporal, multichannel AVHRR data sets for land biosphere studies: Artifacts and corrections, *Remote Sens. Environ., 60*, 35-57, 1997.

Collatz, G. J., J. T. Ball, C. Grivet, and J. A. Berry, Physiological and environmental regulation of stomatal conductance, photosynthesis and transpiration: A model that includes a laminar boundary layer, *Agric. For. Meteorol., 54*, 107-136, 1991.

Czajkowski, K. P., T. Mulhern, S. N. Goward, and J. Cihlar, Validation of the geocoding and compositing system (GEOCOMP) using contextural analysis for AVHRR images, *Int. J. Remote Sens., 18* 3055-3068, 1997a.

Czajkowski, K. P., T. Mulhern, S. N. Goward, J. Cihlar, R. O. Dubayah, and S. Prince, Biospheric environmental monitoring at BOREAS with AVHRR observations, *J. Geophys. Res., 102*, 29,651-29,662, 1997b.

Czajkowski, K. P., S. N. Goward, and H. Ouaidrari, Impact of AVHRR filter function on surface temperature estimation from the split window approach, *Int. J. Remote Sens. 19*, 2007-2012, 1998.

Dang, Q.-L., H. A. Margolis, and G. J. Collatz, Regulation of branch-level gas exchange of boreal trees: Roles of shoot water potential and vapor pressure difference, *Tree Physiol., 17*, 521-536, 1997.

Denning, A. S., I. Y. Fung, and D. Randall, Latitudinal gradient of atmospheric $CO_2$ due to seasonal exchange with land biota, *Nature, 376*, 240-243, 1995.

Fan, S., M. Gloor, J. Mahlman, S. Pacala, J. Sarmiento, T. Takahashi, and P. Tans, A large terrestrial carbon sink implied by atmospheric and oceanic $CO_2$ data and models, *Science, 282*, 442-446, 1998.

Field, C. B., Ecological scaling of carbon gain to stress and resource availability, in *Response of Plants to Multiple Stresses*, edited by H. A. Mooney, W. E. Winner, and E. J. Pell, pp. 35-65, Academic, San Diego, Calif., 1991.

Foley, J. A., I. C. Prentice, and A. Haxeltine, An integrated biosphere model of land surface processes, terrestrial carbon balance, and vegetation dynamics, *Global Biogeochem. Cycles, 10*, 603-628, 1996.

Frolking, S., Sensitivity of spruce/moss boreal forest net ecosystem productivity to seasonal anomalies in weather, *J. Geophys. Res., 102*, 29,053-29,064, 1997.

Gifford, R. M., The global carbon cycle: A viewpoint on the missing sink, *Aust. J. Plant Physiol., 21*, 1-15, 1994.

Goel, N., and W. Qin, Influence of canopy architecture on various vegetation indices and LAI and Fpar: Simulation model results, *Remote Sens. Rev., 10*, 309-347, 1994.

Goetz, S. J., Multi-sensor analysis of NDVI, surface temperature, and biophysical variables at a mixed grassland site, *Int. J. Remote Sens., 18*, 71-94, 1997.

Goetz, S. J., and S. D. Prince, Remote sensing of net primary production in boreal forest stands, *Agric.For. Meteorol. 78*, 149-179, 1996.

Goetz, S. J., and S. D. Prince, Variability in carbon exchange and light utilization among boreal forest stands: Implications for remote sensing of net primary production, *Can. J. For. Res. 28*, 375-389, 1998.

Goetz, S. J., and S. D. Prince, Modeling terrestrial carbon exchange and storage: Evidence and implications of functional convergence in light use efficiency, *Adv. Ecol. Res., 28*, 57-92, 1999.

Goetz, S. J., S. D. Prince, S. Goward, M. Thawley, and J. Small, Satellite remote sensing of primary production: An improved production efficiency modeling approach, *Ecol. Model.*, in press, 1999.

Goulden, M. L., J. W. Munger, S.-M. Fan, B. C. Daube, and S. C. Wofsy, Exchange of carbon dioxide by a deciduous forest: Response to interannual climate variability, *Science,* 271, 1576-1578, 1996.

Goulden, M. L., B. C. Daube, S.-M. Fan, D. J. Sutton, A. Bazzaz, J. M. Munger, and S. C. Wofsy, Physiological responses of a black spruce forest to weather, *J. Geophys. Res., 102*, 28,987-28,996, 1997.

Goulden, M. L., et al., Sensitivity of boreal forest carbon balance to soil thaw, *Science, 279*, 214-216, 1998.

Goward, S. N., and D. Dye, Global biospheric monitoring with remote sensing, in *The Use of Remote Sensing in Modeling Forest Productivity*, edited by H. L. Gholtz, K. Nakane, and H. Shimoda, pp. 241-272, Kluwer Acad., New York, 1997.

Goward, S. N., and K. F. Huemmrich, Vegetation canopy PAR absorbance and the normalized difference vegetation index: An assessment using the SAIL model, *Remote Sens. Environ., 39*, 119-140, 1992.

Goward, S. N., R. H. Waring, and D. G. Dye, Ecological remote sensing at OTTER: Macroscale satellite observations, *Ecol. Appl., 4*, 322-343, 1994.

Gower, S. T., J. Vogel, J. Norman, C. Kulharik, S. Steele, and T. Stow, Carbon distribution and above-ground net primary production of upland and lowland boreal forests in Saskatchewan and Manitoba, Canada, *J. Geophys. Res., 102*, 29,029-29,042, 1997.

Gu, J. and E. A. Smith, High-resolution estimates of total solar and PAR surface fluxes over the BOREAS study area from GOES measurements, *J. Geophys. Res. 102*, 29,685-29,706, 1997.

Hall, F. G., D. E. Knapp, and K. F. Huemmrich, Physically based classification satellite mapping of biophysical characteristics in the southern boreal forest, *J. Geophys. Res., 102*, 29,567-29,580, 1997.

Heinselman, M. L., Fire in the virgin forests of the Boundary Waters Canoe Area, Minnesota, *Quat. Res., 3*, 329-382, 1973.

Holben, B., Characteristics of maximum-value composite images from temporal AVHRR data, *Int. J. Remote Sens. 7*, 1417-1434, 1985.

Huemmrich, K. F., T. A. Black, P. G. Jarvis, J. H. McCaughey, and F. G. Hall, High temporal resolution NDVI phenology from micrometeorological radiation sensors, *J. Geophys. Res.*, this issue.

Hunt, E. R., Relationship between woody biomass and PAR conversion

efficiency for estimating net primary production from NDVI, *Int. J. Remote Sens. 15*, 1725-1730, 1994.

Johnston, A., Estimating standing above-ground biomass with AVHRR visible channel observations, M.A. thesis, Univ. of Md., College Park, 1998.

Kasischke, E. S., N. L. Christensen, and B. J. Stocks, Fire, global warming, and the carbon balance of boreal forests, *Ecol. Appl., 5*, 437-451, 1995.

Keeling, C. D., T. P. Whorf, M. Wahlen, and J. van der Plicht, Interannual extremes in the rate of rise of atmospheric carbon dioxide since 1980, *Nature, 375*, 666-670, 1995.

Keeling, C. D., J. F. S. Chin, and T. P. Whorf, Increased activity of northern vegetation inferred from atmospheric $CO_2$ measurements, *Nature, 382*, 146-149, 1996.

Kimball, J. S., P. E. Thornton, and S. W. Running, Simulating forest productivity and surface-atmosphere carbon exchange in the BOREAS study region, *Tree Physiol., 17*, 589-600, 1997.

Kumar, M., and J. L. Monteith, Remote sensing of plant growth, in *Plants and the Daylight Spectrum*, edited by H. Smith, pp. 133-144, Academic, San Diego, Calif., 1982.

Landsberg, J. J., and R. H. Waring, A generalised model of forest productivity using simplified concepts of radiation-use efficiency, carbon balance and partitioning, *For. Ecol. and Manage., 95*, 209-228, 1997.

Landsberg, J. J., S. D. Prince, P. G. Jarvis, R. E. McMurtrie, R. Luxmore, and B. E. Medlyn, Energy conversion and use in forests: The analysis of forest production in terms of utilisation efficiency (ε), in *Use of Remote Sensing in the Modeling of Forest Productivity*, edited by H. L. Gholtz, K. Nakane, and H. Shimoda, pp. 273-298, Kluwer Acad., San Diego, Calif., 1997.

Lavigne, M. B., and M. G. Ryan, Growth and maintenance respiration rates of aspen, black spruce and jack pine stems at northern and southern BOREAS sites, *Tree Physiol., 17*, 543-552, 1997.

Leemans, R., and W. P. Cramer, *The IIASA Database for Mean Monthly Values of Temperature, Precipitation and Cloudiness on a Global Terrestrial Grid*, Int. Inst. for Appl. Syst. Anal., Laxenburg, Austria, 1991.

Li, Z., L. Moreau, and J. Cihlar, Estimation of photosynthetically active radiation absorbed at the surface, *J. Geophys. Res., 102*, 29,717-29,728, 1997.

Liu, J., J. M. Chen, J. Cihlar, and W. Chen, Net primary productivity distribution in the BOREAS study region from a process model driven by satellite and surface data, *J. Geophys. Res.*, this issue.

Myneni, R. B., G. Asrar, D. Tanre, and B. J. Choudhury, Remote sensing of solar radiation absorbed and reflected by vegetated land surfaces, *IEEE Trans. Geosci. Remote Sens., 30*, 302-314, 1992.

Myneni, R. B., C. D. Keeling, and R. R. Nemani, Increased plant growth in the northern high latitudes from 1981 to 1991, *Nature, 386*, 698-701, 1997.

Nemani, R., L. Pierce, S. Running and S. Goward, Developing satellite-derived estimates of surface moisture status, *J. Appl. Meteorol. 32*, 548-557, 1993.

Potter, C. S., J. T. Randerson, C. B. Field, P. A. Matson, P. M. Vitousek, H. A. Mooney, and S. A. Klooster, Terrestrial ecosystem production: A process model based on global satellite and surface data, *Global Biogeochem. Cycles, 7*, 811-841, 1993.

Prihodko, L., and S. N. Goward, Estimation of air temperature from remotely sensed observations, *Remote Sens. Environ., 60*, 335-346, 1997.

Prince, S. D., A model of regional primary production for use with coarse-resolution satellite data, *Int. J. Remote Sens. 12*, 1313-1330, 1991.

Prince, S. D., and S. J. Goward, Global primary production: A remote sensing approach, *J. Biogeogr., 22*, 815-835, 1995.

Prince, S. D., S. J. Goetz, K. Czajkowski, R. Dubayah, and S. N. Goward, Inference of surface and air temperature, atmospheric precipitable water and vapor pressure deficit using AVHRR satellite observations: Validation of algorithms, *J. Hydrol., 212/213*, 231-250, 1998.

Ranson, K. J., G. Sun, R. H. Liang, N. S. Chauhan, R. J. Cacciola, and O. Kilic, Mapping of boreal forest biomass from spaceborne with synthetic aperture radar, *J. Geophys. Res., 102*, 29,599-29,610, 1997.

Ruimy, A., G. Dedieu, and B. Saugier, Methodology for the estimation of terrestrial net primary production from remotely sensed data, *J. Geophys. Res., 99*, 5263-5283, 1994.

Ruimy, A., P. Jarvis, D. Baldocchi, and B. Saugier, $CO_2$ fluxes over plant canopies and solar radiation: A review, *Adv. Ecol. Res., 26*, 1-51, 1995.

Ruimy, A., G. Dedieu, and B. Saugier, TURC: A diagnostic model of continental gross primary productivity and net primary productivity, *Global Biogeochem. Cycles, 10*, 269-285, 1996.

Running, S. W., and E. R. Hunt, Generalization of a forest ecosystem process model for other biomes, BIOME-BGC, and an application for global-scale models, in *Scaling Physiological Processes*, edited by J. R. Ehleringer and C. B. Field, pp. 141-158, Academic, San Diego, Calif., 1993.

Ryan, M. G., M. B. Lavigne, and S. T. Gower, Annual carbon cost of autotrophic respiration in boreal forest ecosystems in relation to species and climate, *J. Geophys. Res., 102*, 28,871-28,884, 1997.

Salisbury, J. W., and D. M. D'Aria, Emissivity of terrestrial materials in the 8-14 μm atmospheric window, *Remote Sens. Environ., 42*, 83-106, 1992.

Saugier, B., A. Granier, and D. D. Baldocchi, Transpiration of a boreal pine forest measured by branch bag, sap flow and micrometeorological methods, *Tree Physiol., 17*, 511-520, 1997.

Sellers, P. J., J. Cihlar, M. Apps, B. Goodison, D. Leckie, E. Ledrew, P. Matson, and S. Running, Charting the boreal forest's role in global change, *Eos Trans. AGU, 72*(4), 33-40, 1990.

Smith, W. L., Note on the relationship between precipitable water and surface dew point, *J. Appl. Meteorol., 5*, 726-727, 1966.

Steyaert, L. T., F. G. Hall, and T. R. Loveland, Land cover mapping, fire regeneration and scaling studies in the Canadian boreal forest with 1km AVHRR and Landsat TM data, *J. Geophys. Res., 102*, 29,581-29,598, 1997.

Tanré, D., B. N. Holben, and Y. J. Kaufman, Atmospheric correction algorithms for NOAA-AVHRR products: Theory and application, *IEEE Trans. Geosci. Remote Sens., 30*, 231-248, 1992.

Tans, P. P., I. Y. Fung, and T. Takahashi, Observational constraints on the global atmospheric $CO_2$ budget, *Science, 247*, 1431-1438, 1990.

Thawley, M. M., A sensitivity analysis of the GLO-PEM primary production model in a Canadian boreal forest during the 1994 growing season, M.A. thesis, Univ. of Md., College Park, 1998.

Tucker, C. J., C. L. Vanpract, M. J. Sharman, and G. V. Ittersum, Satellite remote sensing of total herbaceous biomass production in the Senegalese Sahel: 1980-1984, *Remote Sens. Environ., 17*, 233-249, 1985.

Waring, R. H., J. J. Landsberg, and M. Williams, Net primary production of forests: A constant fraction of gross primary production?, *Tree Physiol., 18*, 129-134, 1998.

Xiao, X., J. M. Melillo, D. W. Kicklighter, A. D. McGuire, R. G. Prinn, C. Wang, P. H. Stone, and A. Sokolov, Transient climate change and net ecosystem production of the terrestrial biosphere, *Global Biogeochem. Cycles, 12*, 345-360, 1998.

Yang, J., and S. D. Prince, A theoretical assessment of the relation between woody canopy cover and red reflectance, *Remote Sens. Environ., 59*, 428-439, 1997.

S. J. Goetz, S. N. Goward, A. Johnston, S. D. Prince, J. Small, and M. M. Thawley, Laboratory for Global Remote Sensing Studies, Department of Geography, University of Maryland, College Park, MD 20742-8225. (sgoetz@geog.umd.edu)

(Received September 24, 1998; revised April 7, 1999; accepted April 15, 1999.)